Estuarine, Coastal and Shelf Science 153 (2015) 145–155

Contents lists available at ScienceDirect

Estuarine, Coastal and Shelf Science

journal homepage: www.elsevier.com/locate/ecss

Benthic-pelagic uncoupling between the Northern Patagonian Frontal System and Patagonian scallop beds

Bárbara C. Franco [a, *], Elbio D. Palma [b], Mariano H. Tonini [b]

[a] Centro de Investigaciones del Mar y la Atmósfera (CIMA/CONICET-UBA), Intendente Guiraldes 2160 – Ciudad Universitaria. Pabellón II – 2do. Piso, C1428EGA Buenos Aires, Argentina
[b] Departamento de Física, Universidad Nacional del Sur and Instituto Argentino de Oceanografía (IADO/CONICET), Bahía Blanca, Argentina

ARTICLE INFO

Article history:
Received 30 June 2014
Accepted 8 December 2014
Available online 16 December 2014

Keywords:
Northern Patagonian Frontal System
scallop beds
stochastic processes
benthic-pelagic coupling

ABSTRACT

Availability of planktonic food in the bottom is the most important factor to explain the persistence and recurrent localization of Patagonian scallop (*Zygochlamys patagonica*) populations. The establishment of the scallop Sea Bay bed (SBB) has been related with food supply from the Northern Patagonian Frontal System (NPFS). In this article outputs from high resolution numerical models combined with particle tracking methods were used to identify for the first time potential physical mechanisms of food transfer. The model results showed no evidence of benthic-pelagic coupling between the NPFS and the SBB. They also revealed that the dominant instantaneous semidiurnal tidal currents and the mean N–NE flow on the inner-middle Patagonian shelf are the main dynamical mechanisms preventing particles released at the surface of the NPFS to reach the SBB area. Sensitivity studies changing the stochastic numerical method for solving the particle trajectories, the release month and location of the particles, the magnitude of the horizontal turbulent diffusion coefficient and the frequency of the wind forcing did not alter this conclusion significantly.

1. Introduction

The Patagonian continental shelf has high rates of tidal energy dissipation locally induced by large tidal amplitudes, constituting one of the most energetic tidal regimes in the world (Simpson and Bowers, 1981; Glorioso and Flather, 1997; Egbert and Ray, 2001; Palma et al., 2004). Current meter observations indicate that the tidal forcing accounts for more than 90% of the kinetic energy variance in the inner portion of the Patagonian continental shelf ($z < 50$ m) and at least half of the variance in the outer shelf (Rivas, 1997). Strong currents driven by the dominant semidiurnal tide (M_2) inhibit the formation of the seasonal thermocline in some coastal areas of the Patagonian shelf, inducing homogenization of the whole water column even during the spring and summer when the surface heat flux increases (Glorioso, 1987; Rivas et al., 2006).

The Northern Patagonian Frontal System (NPFS, *e.g.*, Sabatini and Martos, 2002; and references therein) presents a NE–SW alignment following the bathymetry between ~42° and 45°S (Fig. 1). Historical hydrographic records indicate a significant interannual variability of the NPFS location (Ehrlich et al., 2000; Sabatini and Martos, 2002). In particular, during 1996 and 1998 an anomalous increase of the water temperature was reported in the region and the NPFS emerged separated in two main fronts, with the spacing between them located near the mouth of the Nuevo Gulf (see Ehrlich et al., 2000). Both branches of the NPFS were located significantly nearest to the coast as compared with the mean position defined by Sabatini and Martos (2002).

The highest rates of tidal energy dissipation occur in the northernmost part of the NPFS (Palma et al., 2004; Tonini et al., 2013). This area is located in the southeastern tip of the Valdés Peninsula extending to the northeast (~42°S) and it has a high-lighted importance as one of the most important frontal areas of the shelf. Along this sector of the NPFS is located the Valdés Front which is associated with high concentrations of chlorophyll-*a*, zooplankton, and fishes (Carreto et al., 1998; Sabatini and Martos, 2002; Acha et al., 2004). In the southernmost part of the NPFS (~43°–45°S) rates of tidal energy dissipation are not so high. This area is related with spawning and nursery areas of the anchovy (*Engraulis anchoita*) and hake (*Merluccius hubbsi*), two important commercial fish species of Argentina (Ehrlich and Ciechomski,

* Corresponding author.
E-mail addresses: barbara.franco@cima.fcen.uba.ar (B.C. Franco), uspalma@criba.edu.ar (E.D. Palma), mtonini@criba.edu.ar (M.H. Tonini).

http://dx.doi.org/10.1016/j.ecss.2014.12.006
0272-7714/

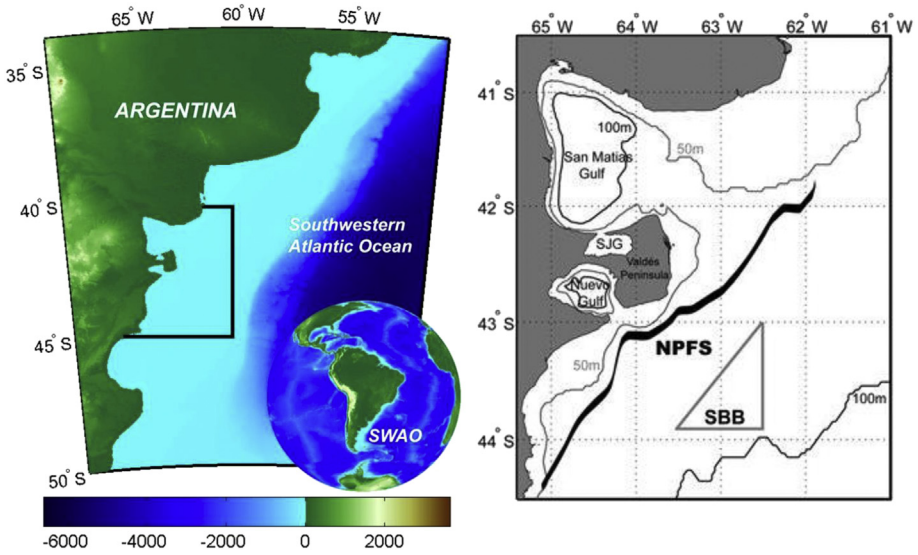

Fig. 1. Study area located in the Southwestern Atlantic Ocean (SWAO, left panel); Schematic illustration of the NPFS mean position (*e.g.*, Sabatini and Martos, 2002) and the Sea Bay bed area (SBB, dark gray polygon) (right panel). The North Patagonian Gulfs (Nuevo Gulf -NG-, San Matías Gulf -SMG-, and San Jose Gulf -SJG-) and the 50 and 100 m isobaths are shown.

1994). Other authors also indicated that the main spawning period of adult hake occurs during spring and summer in the stratified side of the frontal area (NPFS) along 43°–45.5°S (Pájaro et al., 2005).

Previous studies have suggested that the establishment of the Patagonian scallop Sea Bay bed (SBB, ~43.9°S and ~62.5°–63.5°W) (Fig. 1), occurs matching the NPFS location (see Bogazzi et al., 2005; Ciocco et al., 2006). Availability of planktonic food in the bottom is the most important factor to explain the persistence and recurrent localization of Patagonian scallop populations (Orensanz et al., 2006). The NPFS has been suggested to be able to supply planktonic food towards the SBB through benthic-pelagic coupling processes; however, the physical processes which could induce such coupling between the NPFS and SBB are not known. A high interannual variability in the recruitment of the species in the SBB is reported by Ciocco et al. (2006). Therefore, improving our knowledge about the dynamics and variability of the NPFS is crucial to improve fisheries management and overfishing prevention strategies, and to provide a better understanding about fluctuations in the recruitment of a wide group of marine species.

The primary aim of this study is to investigate the physical processes which could induce benthic-pelagic coupling between the NPFS and SBB. To address this investigation we will employ results from idealized and realistic numerical models combined with stochastic Lagrangian particle tracking methods. In Section 2, the numerical models and the calculations are described. Section 3 characterizes the dynamics and variability of the NPFS at semidiurnal and intra-seasonal scales, and analyzes how the dynamics of this frontal system and its variability affect particles transport. Some conclusions follow in Section 4.

2. Material and methods

2.1. Hydrodynamic numerical models

To analyze the dynamics and variability of the NPFS we employed idealized and realistic numerical simulations based on the Regional Ocean Modeling System (ROMS, Shchepetkin and McWilliams, 2005).

2.1.1. Idealized numerical model of a tidal frontal system

The study of Bogazzi et al. (2005) suggests that the NPFS would maintain the existence of the SBB by supplying planktonic food from the surface. However, Simpson (1998) argued that in a tidally-controlled environment horizontal particle movements of more than ~10–15 km from the average frontal position are unlikely. The purpose of the idealized model is precisely to show the strength of this argument in a controlled experiment resembling the Patagonian shelf environment using a quasi two-dimensional version of ROMS.

The model has a periodic domain open in the north-south direction and an idealized continental shelf with 400 km (W–E). The parameterization of vertical mixing is calculated using the Large–McWilliams–Doney (LMD) turbulent closure scheme, with higher vertical resolution at the top and bottom layers (Large and Gent, 1999). The spatial resolution of the horizontal grid is of about 6 km. The semidiurnal tidal component (M_2) was imposed at the lateral open side (E) of the model domain with an amplitude of 0.75 m. This tidal amplitude generates a mean sea level rise of 1.5 m in the coast during the high tide according observations reported previously near the Valdés Peninsula. At the same lateral open side (E) of the model domain a combination of radiation and advection conditions is used (Marchesiello et al., 2001). Seasonal surface heat fluxes for the Patagonian region are calculated as recommended by Rivas (1994) and incorporated in the model through a parameterization following the formulation of Barnier (1998). A wind stress of 0.1 Pa with uniform westward direction (*i.e.*, simulating the predominant offshore wind) is imposed at the surface. The model was run during 3 years were a statistical steady state of energy balance was achieved. The outputs of the model for the last year of simulation were analyzed.

2.1.2. Realistic numerical model of the NPFS

For our realistic experiments outputs (three dimensional currents and vertical diffusivity fields) from a high resolution hydrodynamic model (ROMS, 3-D) of the North Patagonian region were used (Tonini et al., 2013). The resulting flow patterns and tracer fields (temperature and salinity) obtained with this model were analyzed and validated against the available observations in Tonini et al. (2013); here only a brief summary is given. The spatial resolution of the grid is variable, with maximum resolution (~1 km) into the gulfs. In the vertical the model equations were discretized in 20 sigma levels, with higher vertical resolution at the top and bottom layers. The bathymetry is based on digitized nautical charts. At the lateral open boundaries of the model they impose tidal amplitudes

and phases of six constituents (M_2, S_2, N_2, O_1, M_1 and P_1) interpolated from a global tidal model (TPOX6, Egbert et al., 1994). The model was forced at the sea surface with the monthly mean climatological wind stress (τ^w) from the SCOW 8-year Quikscat climatology of ¼ degree spatial resolution (Risien and Chelton, 2008) and heat fluxes from Rivas (1994) and freshwater fluxes from COADS.

2.2. Particle tracking models

A high concentration of chlorophyll-*a* is associated with the NPFS mainly during the spring and early summer (Acha et al., 2004). The Patagonian scallop is primarily a suspension filter feeder of phytoplankton (Schejter et al., 2002), although the species may also feed on more degraded suspended organic matter (Mauna et al., 2011). Therefore, our study is aimed to investigate the benthic-pelagic coupling processes occurring in the NPFS during the months from September to December. To perform a comparative study on the semidiurnal and intra-seasonal variability of the NPFS obtained with the idealized and the realistic model, the outputs of both hydrodynamic models for the months of September to December recorded every 1 h of simulation were used. The Lagrangian stochastic model was used to perform the numerical experiments of particle tracking using the horizontal and vertical velocity components and the vertical diffusivity coefficient taken from the models at each 1 h. The stochastic displacement of the particles was calculated using a time step of 2 s for the idealized model and 4 s for the realistic model experiments. This small time step is recommended to carry out Lagrangian stochastic simulations to avoid artificial vertical accumulations of particles in situations involving nonhomogeneous vertical diffusivity (see Ross and Sharples, 2004).

2.2.1. Lagrangian stochastic model

The Lagrangian Stochastic (LS) modeling theory has been the basis of larval dispersal models and Individual Based Models (IBMs). The use of such models in biophysical modeling studies has increased broadly (Werner et al., 1996, 2001; Siegel et al., 2003). Usually, the Lagrangian approach follows particles in space at each time step and their movement is modeled with a Stochastic Differential Equation (SDE), known as a Random Displacement Model (RDM). The RDM was derived from the Langevin equation model and it is consistent with the advection–diffusion equation through a probability distribution function (Fokker–Planck equation; see Rodean, 1996). The RDM for steady nonhomogeneous diffusivity in the vertical coordinate (z) is:

$$dz = \left[w(z,t) + \frac{\partial K(z,t)}{\partial z}\right]dt + [2K(z,t)]^{1/2}dW(t) \quad (1)$$

where dz is the change in the vertical position of the particle, the first term in the right-hand-side is the drift component [composed by advection, $w(z, t)$ and a drift correction], and the second term is the stochastic component of the SDE. K is the turbulent diffusion coefficient and $dW(t)$ is one incremental Wiener process. The Wiener process is a continuous, Gaussian, and Markov process which is consistent with a diffusion model (Rodean, 1996). Gardiner (1983) presented the interpretation of an incremental Wiener process $dW(t)$, in which each increment is independent, and a Gaussian random variable with mean $E(dW_n) = 0$ and variance $E((dW_n)^2) = dt$. Several oceanographic studies used distinct formulations of the RDM, particularly with respect to the calculation of the diffusion (or mixing) coefficient $K(z)$ in the stochastic component of the SDE (Hunter et al., 1993; Visser, 1997; Ross and Sharples, 2004; North et al., 2005, 2006; Ross, 2006). According to Hunter et al., 1993, an improvement in the formulation of the RDM can be achieved by computing the mixing coefficient at an intermediate point of the (vertical) space interval. Regrouping terms in (1) the new RDM (*i.e.*, Hunter/Visser approximation) would be:

$$dz = \left[w(z,t) + \frac{\partial K(z,t)}{\partial z}\right]dt + \{2K[z + 1/2\partial K(z,t)/\partial z, t]\}^{1/2}dW(t) \quad (2)$$

Visser (1997) demonstrated that Eq. (2) is also equivalent to the (Eulerian) advection–diffusion equation. However, the formulation of this equation requires the use of an interpolation scheme to calculate the vertical mixing coefficient at an intermediate point. Following the formulation used by Hunter/Visser a model of larval transport was developed (LTRANS, Larval Transport Lagrangian Model) at the University of Maryland (Schlag et al., 2008). The model is configured to predict the movement of particles due to advection, turbulence, and larval behavior for biophysical studies. This off-line particle tracking model is endowed with a sophisticated scheme of interpolation and smoothing of the vertical diffusivity field (Tension Splines). The 'tension spline' scheme does not add inflection points, as simple 'spline' methods. Moreover, the scheme preserves the monotonicity and convexity of the data field. Properly designed interpolation schemes are important in the presence of nonhomogeneous diffusivity fields since the drift and diffusion coefficients of a SDE needs to be sufficiently smooth for the transition probability of the Markov process to satisfy the Fokker–Planck equation (Kloeden and Platen, 1999).

Usually studies using coastal circulation models regarded the coefficient of horizontal diffusivity (K_h) either constant or null in the simulations. However, in a region with eddies or strong tidal currents that induce intense turbulent mixing the stochastic behavior (sub-grid scale) might also be considered in the horizontal for particle tracking. LTRANS contains a provision for a horizontal turbulent coefficient to simulate horizontal diffusion using a Gaussian random flight process with additional displacements (dx and dy) in the form of a "naive" random walk (Visser, 1997):

$$(dx, dy) = (2K_h)^{1/2}dW(t) \quad (3)$$

In this work we analyzed differences in the particle dispersion behavior when adding a horizontal random-walk with two values of K_h (1 and 50 m^2/s) which are reasonable for the study region (Ledwell et al., 1998).

2.2.2. Numerical solutions to RDM

The simplest and usually employed numerical scheme to approximate the numerical solutions of the RDM is the Euler method, also known as Euler–Maruyama (EM). This scheme has a strong order of convergence $\gamma = 0.5$ and weak order of convergence $\beta = 1$. Numerical methods with higher order of convergence in the strong sense are used in stochastic problems when higher precision in the integration of each particle path is required (*i.e.*, each simple Wiener path). A higher order stochastic numerical scheme obtained by truncation of the stochastic Itô-Taylor series is the Milstein method (*e.g.*, Milstein, 1974, ML). Milstein higher order method present strong convergence ($\gamma = 1$) to solve Itô-SDEs.

Some studies have shown how high order (in the strong sense) stochastic schemes are important to better solve boundary conditions when the RDM is applied (Stijnen et al., 2006; Charles et al., 2009). If the numerical solutions do not solve well the particle's trajectories near the boundaries of the model domain some particles may be reflected by boundary conditions. In this work we implemented the LTRANS model to compare the EM method, the standard Hunter–Visser approach (LT) and the higher order

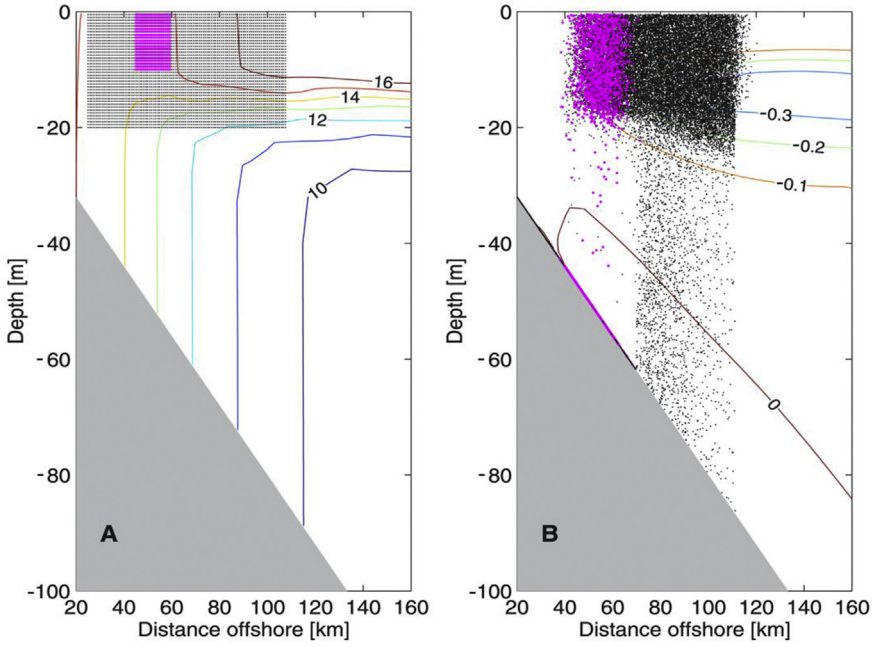

Fig. 2. (**A**) Temperature (°C) section along the idealized shelf and location of the particles released at the start of the simulation (black dots). (**B**) Vertical gradient of temperature (°C/m) section and location of the particles after 10 days of particle tracking simulation. Particles released from the area of surface frontal variability and above the pycnocline are shown (magenta dots). (For interpretation of the references to color in this figure legend, the reader is referred to the web version of this article.)

numerical scheme of ML for solving the classical formulation of the RDM (Eq. (1)). Furthermore, we compare the numerical solutions for both RDM formulations (Eqs. (1) and (2)). The discrete form of the RDM formulations for the proposed integration schemes is given in Appendix A.

2.2.3. Statistical analysis

Particles were tracked, as described above to characterize each monthly condition; their ending positions were used in defining a 2-D dispersal kernel (ellipse of dispersion). A Principal Component Analysis (PCA) was used to compute the ellipses of dispersion. The distortion of a particle group is quantified by a horizontal covariance matrix, the components of which account for the covariance between particle displacements relative to their center of mass. The dispersion is extreme in the direction of the semi-major axis; whereas its length gives the root-mean square (rms) displacement (Sentchev and Korotenko, 2007). This approach was used to investigate the following effects on the larval dispersion: (i) larval release month (September through December), (ii) stochastic numerical method (EM, LT, and ML) and (iii) horizontal diffusivity (K_h).

3. Results and discussion

3.1. Idealized tidal frontal system

During early October the tidal frontal system showed a vertically well mixed and homogenized coastal area until ~40 km offshore and a strong offshore thermal stratification (Fig. 2A and B). The surface thermal front recorded a progressive displacement towards the coast until late October, which was induced by surface seasonal heat fluxes. Frontal movements during November and December vary only in the semidiurnal cycle (not shown). Displacements of the tidal fronts from their mean positions may result from simple tidal advection or adjustments due to changes in the stirring and heating rates (Simpson, 1981). The intra-seasonal displacement of the surface thermal front recorded is of ±35 km and it occurs from the last 10 days of September, when the structure of the tidal frontal system is already characterized and stratified, until late October. In addition, the model recorded oscillations in the semidiurnal cycle of ~8–10 km. In the semidiurnal scale predictions of numerical models are a very useful tool to study the variability of the tidal fronts (Simpson, 1998). The model results agree with satellite derived sea surface temperature observations indicating a displacement of some tens of km of the Valdés Front between spring and summer (Pisoni et al., 2014). The variability recorded in the position of the surface thermal front therefore highlights that the surface heat cycle is the dominant forcing on the spatial variability of a typical tidal front in the Patagonian region.

The influence of the semidiurnal tidal advection on the thermal structure of the front is showed to occur in both the bottom and the surface mixed layers (see Temp_OCTm2.avi in Supplementary Material). This movie reproduces a one day simulation of the idealized model for early October. The semidiurnal tidal oscillations induce horizontal displacements of the surface front. Therefore, the semidiurnal vertical cycle of stratification also induces vertical mixing and transport of the particles concentrated in the area of surface frontal variability. The periodic semidiurnal breakdown of the vertical stratification in the area of surface frontal variability may induce particles initially located at the bottom of the surface mixed layer to be transported towards the bottom mixed layer. Simpson and Souza (1995) reported that semidiurnal oscillations in the stability of the water column are forced mainly by tidal advection when horizontal movements interact with vertical density gradients generating disturbances in the stratification.

Supplementary video related to this article can be found at http://dx.doi.org/10.1016/j.ecss.2014.12.006.

The influence of semidiurnal tidal oscillations on transporting particles initially located in the surface of the frontal area was investigated with a particle tracking experiment. A total of 4000 particles were released along a broad area (~80 km) through the idealized shelf from the surface to 20 m depth (Fig. 2A). A set of 10

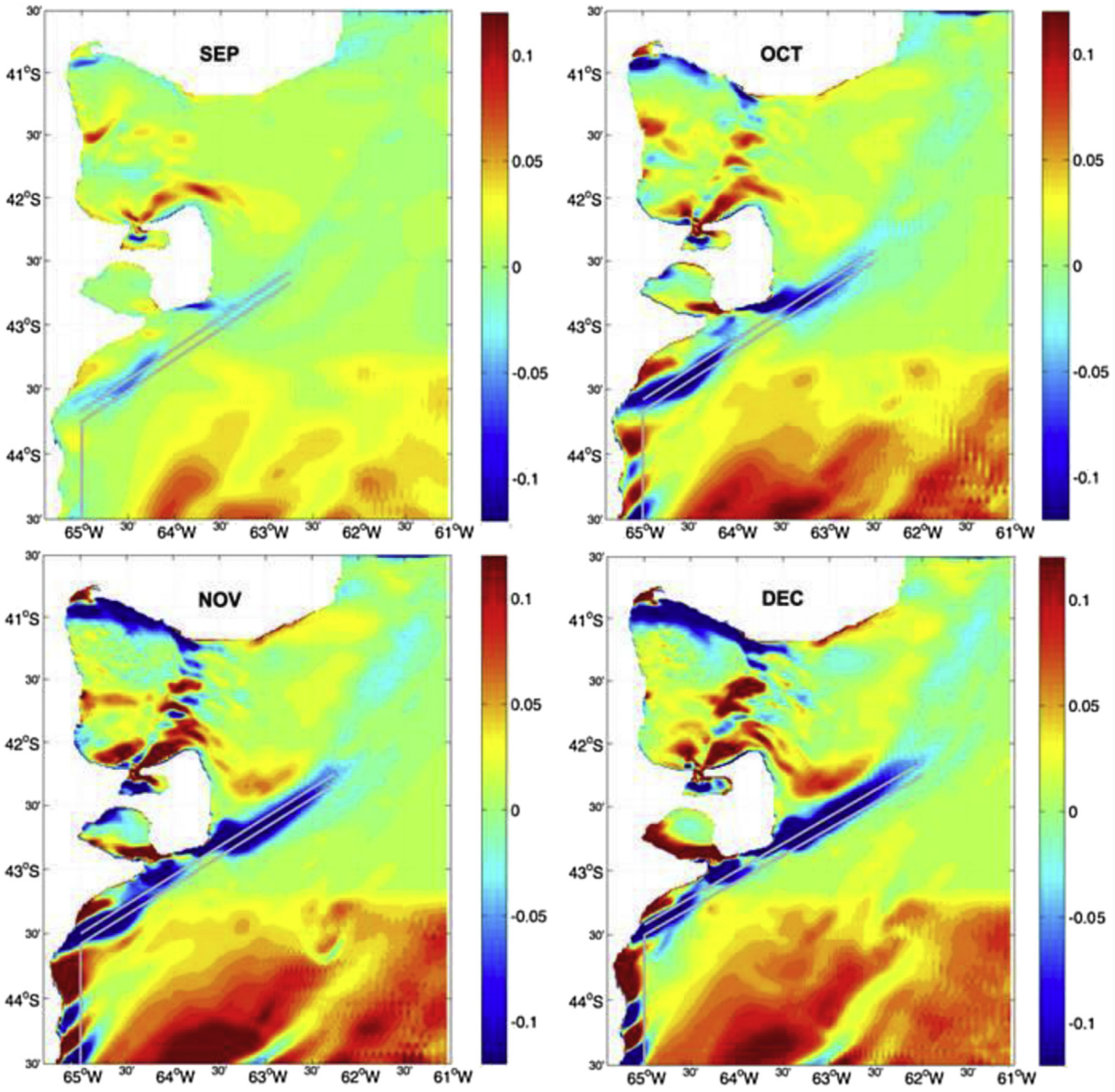

Fig. 3. Monthly meridional gradient of surface temperature [gyTSM (°C/km)]. The monthly mean position of the NPFS at high (nearest the coast) and low tides are indicated (light gray lines).

distinct particle tracking simulations were performed for a total simulation period of 10 days. Particles released from the area of surface frontal variability and above the pycnocline (0–10 m) are shown in Fig. 2A (magenta dots). LTRANS (LT approach) was configured to stop any particle that reaches the bottom.

The statistical result of the average positions (x, z) of the particles at the last time step of the set of 10 distinct simulations showed that all particles released from the vertically homogenous coastal area of the tidal front reach the bottom. The particle tracking results showed that 31% of the particles released from the area of surface frontal variability (located initially above the pycnocline) reach the bottom matching approximately the area of frontal variability in the surface. Only 5% of the particles released from the stratified area reach the bottom (Fig. 2B). The largest settlement in the bottom occurs from the mixed coastal area to the offshore position of the bottom front of the tidal frontal system.

3.2. Northern Patagonian Frontal System (NPFS)

The intra-seasonal and semidiurnal variability of the NPFS was characterized mainly by calculating the meridional gradient of sea surface temperature from the realistic model results (gyTSM, Fig. 3). The meridional gradient of sea surface temperature is stronger than the zonal gradient in the study area and it highlights the presence of two major thermal fronts along the NPFS. Furthermore, the gyTSM matched well with the results obtained by the total gradient of sea surface temperature in those different months (see Franco, 2013). This methodology (gyTSM) showed the presence of two main fronts with negative thermal gradients which are separated just in front of the mouth (E–NE) of the Nuevo Gulf. Such negative thermal fronts have distinct extensions of frontal variability and as we will show later these differences are also reflected in the particle transport dynamics. The monthly mean

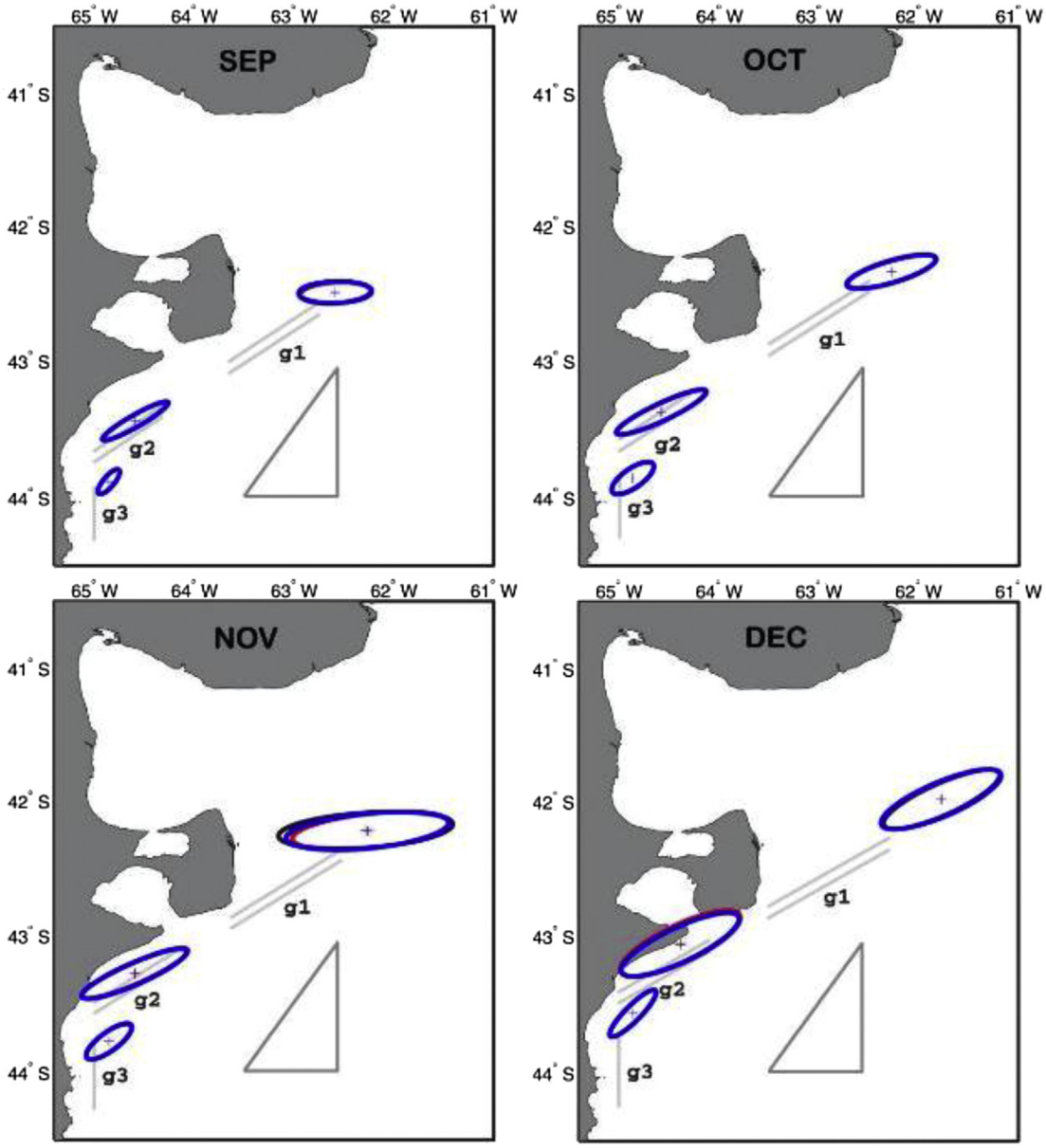

Fig. 4. Location of dispersal ellipses (2D) of the particles released from the lines of monthly variability areas for three distinct fronts identified along the NPFS (light gray lines labeled as **g1**, **g2**, and **g3**). The experiments used $K_h = 1$ m^2/s and ellipses are shown according the numerical method employed: EM (black), LT (red), and ML (blue). The polygon configured for settlement of particles (SBB) is illustrated by dark gray lines. (For interpretation of the references to color in this figure legend, the reader is referred to the web version of this article.)

position of the NPFS was characterized based on the observation of gyTSM during semidiurnal tidal cycles. The area of monthly frontal variability was established between the mean positions of the high and low tides, taking into account the first and last semidiurnal cycle of each month. These positions are indicated in Fig. 3 for each month (gray lines). The monthly mean position of the NPFS has large intra-seasonal variability, mainly north of ~43.75°S. The most pronounced thermal gradients (gyTSM) between latitudes ~43.75°–44.5°S are observed almost aligned to the coast and the frontal variability occurs mainly in the semidiurnal period (~8–10 km). In the meridional direction this gyTSM appear as a sequence of positive and negative gradients due to the contours of the coast. NPFS monthly mean positions at high and low tides which are indicated by two parallel lines north of ~43.75°S and by one line toward 44.5°S (65°W) delimit the areas of particles release for each month, respectively.

3.3. NPFS particle dispersal and benthic-pelagic coupling processes

Commercial trawl fishery for scallops recorded during 1989 and 1995–2003 were concentrated near the area defined as SBB (see Bogazzi et al., 2005). For our experiments a major area of occurrence of the scallop, which correspond mainly to the benthic bed area, was considered to delimit a polygon illustrated in Fig. 1 and figures shown hereafter. This polygon was set up for the settlement of the particles that reach the bottom in this area in each numerical experiment. However, particles reaching the bottom outside of this polygon are free to move with the currents. To characterize the dispersion in the upper mixed layer a total of 800 particles were released at the surface ($z = 0$ m) from the area of frontal variability of the Valdés Front (**g1**), 600 particles from the front located between the mouth of the NG to ~43.75°S (**g2**) and 500 particles from the front located between ~43.75°S and 44.5°S (**g3**). Lines

indicating the locations of the releases are shown by light gray in Fig. 4. Only particles located in the surface and upper mixed layer ($0 < z < 10$ m) were considered to calculate the PCA and the configuration of the ellipses of dispersion (2D). Our statistical results were calculated by reproducing a set of 10 distinct simulations for each numerical method (EM, LT, and ML). The configuration of the ellipses of dispersion (2D) involves mean positions (x, y) of each particle for the last 24 h of each monthly simulation. The mean positions (x, y) obtained for each particle in each one of the 10 distinct trials of a single experiment were averaged statistically. Then, the ellipses of dispersion for each month can be compared and allow us to perform a sensibility analysis by changing the values of the coefficient of horizontal diffusivity and the stochastic numerical scheme used in each experiment. In Fig. 4 are shown the results for the experiments using $K_h = 1$ m^2/s and in Fig. 5 the $K_h = 50$ m^2/s. These statistical results (ellipses of dispersion) indicate the areas of highest concentration of particles located in the euphotic zone after each month of simulation. Each one of these areas should represent hence areas of high quantity of planktonic food (*e.g.*, phytoplankton and organic detritus) originated in the fronts.

The strong circulation induced by the instantaneous tide in this coastal region induces a weaker horizontal dispersion of the particles from their front of release. We observed a higher dispersion of the particles towards the coast and this evidence is stronger when the NPFS is closer to the coast. For instance, in December a higher

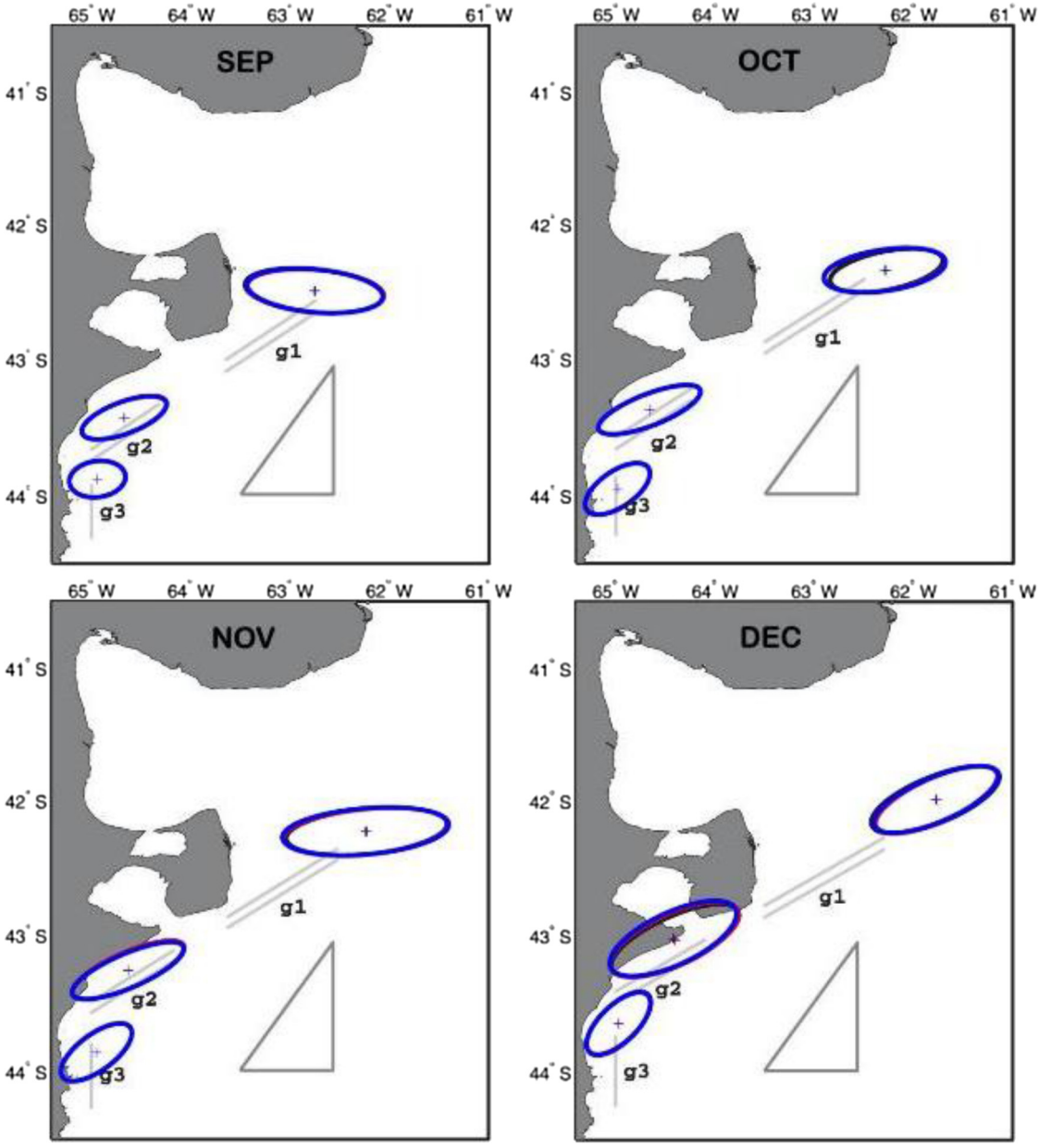

Fig. 5. Location of dispersal ellipses (2D) of the particles released from the lines of monthly variability areas for three distinct fronts identified along the NPFS (light gray lines labeled as **g1**, **g2**, and **g3**). The experiments used $K_h = 50$ m^2/s and ellipses are shown according the numerical method employed: EM (black), LT (red), and ML (blue). The polygon configured for settlement of particles (SBB) is illustrated by dark gray lines. (For interpretation of the references to color in this figure legend, the reader is referred to the web version of this article.)

number of particles flowed into the NG, SMG, and SJG. The inflow of particles into the North Patagonian gulfs was evidenced mainly in November and December and hence the larger is the length of the ellipses resulting from the particles released from the front **g2**. This result is shown in the experiments using both values of K_h (Figs. 4 and 5). The dispersion of some particles into the SMG and SJG changed the main direction (NE) of the ellipses configured for the particles released from the Valdés Front (**g1**) in distinct months (Figs. 4 and 5). The ellipses configured for the particles released from the fronts **g2** and **g3** agree with the general pattern of circulation on the Patagonian shelf, forced mainly by residual tidal flow and the surface Ekman transport, which generates a predominant flow in the direction N–NE (Tonini et al., 2013). In neither of the months the bulk of the particles were dispersed towards the area delimited by the polygon. A higher K_h induced larger horizontal dispersion (rms) and hence a larger length of semi axes of the ellipses. However, this change did not affect significantly the main directions of the particles dispersion from the distinct fronts (the major semi axis direction).

Our results indicate that particles released from the NPFS are not dispersed towards the Patagonian scallop SBB. In coastal areas surrounding the NPFS the dominant circulation of instantaneous semidiurnal tide and the mean flow towards N–NE on the inner-middle shelf cannot transport particles released in the NPFS towards the bed. According to Bogazzi et al. (2005) the area of the bed, located mainly where the largest concentration of fishing effort is recorded occurs near ~43.9°S and 63°–63.5°W corresponding to an approximate distance of 170–200 km from the

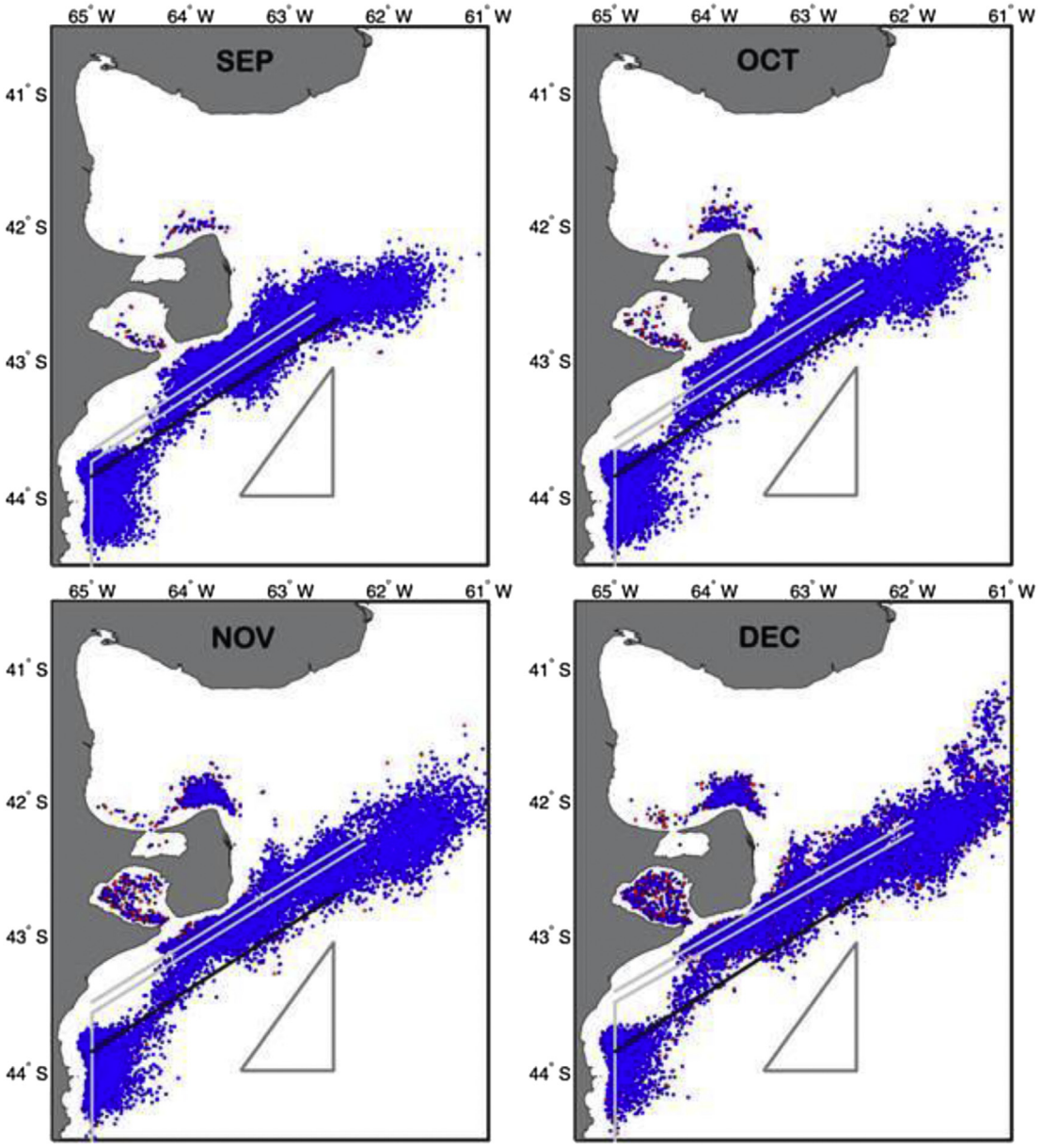

Fig. 6. Location of the positions (x, y) of the particles released from the lines of monthly variability area of the NPFS. Particles located in the bottom mixed layer (depth < 40 m) at the last day of simulation for each month are shown. The positions are the mean location from 10 trials for each numerical method: EM (black dots), LT (red dots), and ML (blue dots). An additional line of release located in the stratified area of the NPFS is shown by a black line. The polygon configured for settlement of particles (SBB) is illustrated by dark gray lines. (For interpretation of the references to color in this figure legend, the reader is referred to the web version of this article.)

coast. Our model results showed that the NPFS is located near the coast at this latitude (~43.9°S) and the frontal position is oscillating mainly at the semidiurnal cycle near approximately 65°W (~30 km from the coast).

In the last step of the numerical experiments we aimed to characterize the coverage area of the particles released from the surface ($z = 0$ m) of the area of monthly frontal variability of NPFS and that reach the bottom mixed layer ($z < 40$ m). The objective of this experiment was to investigate the possible benthic-pelagic coupling processes occurring in the study area. A total of 4000 particles were released at the surface ($z = 0$ m) from the area of frontal variability of the NPFS. It includes a release line located over the stratified side of the front (see Fig. 6). The experiments also assessed the effect of choosing a different stochastic numerical method (EM, LT, and ML) on the particle's horizontal dispersion. The statistical results were also calculated by reproducing a set of 10 distinct simulations for each numerical method. Monthly mean positions of each particle (x, y) and for each numerical method were calculated by the average of the positions during the last 24 h of each simulation in each one of the 10 distinct simulations. Results of the experiments that used $K_h = 50$ m^2/s for the distinct numerical methods are shown by different colors in Fig. 6. The higher value of K_h was selected to investigate the possible benthic-pelagic connection between the NPFS and the SBB in a situation of higher horizontal diffusivity. Higher differences in horizontal dispersal of the particles released using the different numerical stochastic methods were observed mainly over the NG and deeper areas of the SMG. However, in none of the 240 numerical experiments simulated in this study some of the particles approached the polygon representing the area of occurrence of the SBB, during the entire time of the simulations.

In tidal shelf fronts the wind is important inducing mixing mainly in the coastal and homogenous side of the front. Our experiments were forced with climatological mean winds and there might be concern about the effect of high frequency (*i.e.*, daily) wind variability on the particle's behavior. To examine this influence we have reproduced the experiment of particles released from the lines of monthly variability area of the NPFS during September, when the tidal front is located more offshore. Daily wind stress for 2010 obtained from the ERA-Interim reanalysis database (Dee et al., 2011) was imposed to conduct our experiments. A total of 4000 particles were released at the beginning of September and followed during 30 days. The dispersion of the particles reported from 10 trials at the last day of simulation (not shown) indicated that no particle could reach the SBB. Ancillary experiments conducted releasing particles in the coastal zone also indicated no trend of the particle displacements to follow an offshore path towards the SBB. These results further support our conclusion that the strong tidal currents characteristic of this region can be more important than high-frequency wind variations.

It has been shown that differences in the modeling of the vertical stochastic behavior of particle tracking algorithms can substantially modify the horizontal particle trajectories (Stijnen et al., 2006). To quantify this behavior we compared the vertical displacements of particles released from the high tide line south of the Valdés Front in our last experiment for the month of December (Fig. 6) using the different numerical approaches (EM, LT and ML). Although the standard deviation of the vertical movement exceeds 10 m in approximately half of the tracked particles (not shown) the average horizontal displacements (dispersal ellipses) did not show significant differences (Figs. 4 and 5).

Individual phytoplankton behavior surely has some influence on its dispersion. We do not have available data to consider the upward swimming speed or different settling velocities (influenced by the size and density) for the species of phytoplankton concentrated in the NPFS. However the magnitude of upward swimming speed for several species of phytoplankton is in order of 10^{-4} m/s (Durham et al., 2009), while vertical velocities in the Patagonian region are mainly in order of 10^{-3} m/s. Then active phytoplankton behavior does not appear to be a significant factor enough to change the conclusion of our study. Such issues, however, can be explored in future works.

Biophysical modeling can be an important tool with which to track larvae from spawning to settlement and to infer patterns of larval dispersal (Werner et al., 2001). A previous study of Edwards et al. (2007) provides a baseline in quantifying and understanding larval dispersal on the inner- and mid-shelf of the central southeast US continental shelf. The authors employed a 3D circulation model combined with Lagrangian particle-tracking to follow particles and to calculate the dispersal kernels (2D). Off-line particle-tracking simulations were also analyzed to determine resulting changes in larval dispersal and connectivity on the central Chilean coast (Aiken et al., 2011). None of them however, have used particle-tracking methods to determine benthic-pelagic coupling processes by comparing the dispersal of the planktonic food and the location of a marine benthic bed. This approach is a useful baseline to understand the productivity and survival of benthic species, as well as fluctuations in their distribution and abundance.

4. Conclusions

Particle tracking studies driven with flow fields generated by high resolution numerical models and state-of the art stochastic models did not support any evidence of a benthic-pelagic coupling between the NPFS and the nearby SBB. Sensitivity studies changing the stochastic numerical method for solving the particle trajectories, the release month (*i.e.*, initial stratification) and location (frontal and coastal) of the particles, the frequency of the wind forcing (climatological and daily) and the magnitude of the horizontal turbulent diffusion coefficient did not alter this conclusion significantly. The robustness of the numerical results is related to the dominant presence of strong instantaneous semidiurnal tidal currents in the study area which prevented particles released at the surface of the NPFS to reach the SBB sector at the bottom.

The dominant N–NE mean flow over the inner-middle Patagonian shelf suggests that food (*i.e.*, phytoplankton and organic detritus) should arrive at the SBB main area from the S–SW direction. Rivas et al. (2006) recorded a high concentration of chlorophyll-*a* over the inner-middle shelf at latitude of the fronts **g2** and **g3** (Fig. 4). The occurrence of Patagonian scallop near the SBB area could be sustained by this high concentration of chlorophyll-*a* (phytoplankton) that occurs in the inner-middle shelf covering the area of the bed during spring and summer. This hypothesis is also supported by a wide distribution of the species reported around the SBB main area and offshore the NPFS position in distinct years (see Fig. 7, Sabatini and Martos, 2002; Fig. 4, Bogazzi et al., 2005).

Acknowledgments

This article was strongly benefited from the comments and suggestions of two anonymous reviewers and interactions with the ECSS Editor. BCF was supported by a Doctoral Scholarship provided by CONICET, Argentina. The work was carried out with the aid of a grant from the Inter-American Institute for Global Change Research (IAI) SGP2076, which is supported by the US National Science Foundation (Grant GEO-0452325). E.D. Palma acknowledges the financial support from Agencia Nacional de Promoción Científica y Tecnológica (PICT12–0467), Universidad Nacional del Sur (24F044), and MINCyT/CONAE (001).

Appendix A

Itô-Euler–Maruyama (EM):

$$z^{n+1}(t) = z^n(t) + \left[w(z,t) + \frac{\partial K(z,t)}{\partial z}\right]\mathrm{d}t + [2K(z,t)]^{1/2}\mathrm{d}W(t) \quad (1)$$

Itô-Milstein (ML):

$$z^{n+1}(t) = z^n(t) + \left[w(z,t) + \frac{\partial K(z,t)}{\partial z}\right]\mathrm{d}t + [2K(z,t)]^{1/2}\mathrm{d}W(t) + \frac{1}{2}[2K(z,t)]^{1/2}\frac{\partial [2K(z,t)]^{1/2}}{\partial z}\left\{[\mathrm{d}W(t)]^2 - \mathrm{d}t\right\} \quad (2)$$

The discrete form of the modified formulation for the Eq. (2) is: Hunter/Visser (LT):

$$z^{n+1}(t) = z^n(t) + \left[w(z,t) + \frac{\partial K(z,t)}{\partial z}\right]\mathrm{d}t + \{2K[z + 1/2\partial K(z,t)/\partial z, t]\}^{1/2}\mathrm{d}W(t) \quad (3)$$

References

Acha, E.M., Mianzan, H.W., Guerrero, R.A., Favero, M., Bava, J., 2004. Marine fronts at the continental shelves of austral South America. Physical and ecological processes. J. Mar. Syst. 44, 83–105.

Aiken, C.M., Navarrete, S.A., Pelegrí, J.L., 2011. Potential changes in larval dispersal and alongshore connectivity on the central Chilean coast due to an altered wind climate. J. Geophys. Res. Biogeosci. 116, G04026. http://dx.doi.org/10.1029/2011JG001731.

Barnier, B., 1998. Forcing the ocean. In: Ocean Modeling and Parameterization. Springer, Netherlands, pp. 45–80.

Bogazzi, E., Baldoni, A., Rivas, A., Martos, P., Reta, R., Orensanz, J.M., Lasta, M., Dell'Arciprete, P., Werner, F., 2005. Spatial correspondence between areas of concentration of Patagonian scallop (*Zygochlamys patagonica*) and frontal systems in the southwestern Atlantic. Fish. Oceanogr. 14, 359–376.

Carreto, J.I., Montoya, N.G., Cucchi Colleoni, A.D., Akselman, R., 1998. *Alexandrium tamarense* blooms and shellfish toxicity in the Argentine Sea: a retrospective view. In: Reguera, B., Blanco, J., Fernandez, M., Wyatt, T. (Eds.), Harmful Algae, pp. 131–134.

Charles, W.M., van den Berg, E., Lin, H.X., Heemink, A.W., 2009. Adaptive stochastic numerical scheme in parallel random walk models for transport problems in shallow water. Math. Comput. Model. 50, 1177–1187.

Ciocco, N.F., Lasta, M.L., Narvarte, M., Bremec, C., Bogazzi, E., Valero, J., Orensanz, J.M., 2006. Fisheries and aquaculture: Argentina. In: Shumway, S.E. (Ed.), Scallops: Biology, Ecology and Aquaculture, second ed. Elsevier, Amsterdam, pp. 1251–1292.

Dee, D.P., Uppala, S.M., Simmons, A.J., Berrisford, P., Poli, P., Kobayashi, S., Andrae, U., et al., 2011. The ERA-Interim reanalysis: Configuration and performance of the data assimilation system. Q. J. Roy. Meteorol. Soc. 137 (656), 553–597.

Durham, W.M., Kessler, J.O., Stocker, R., 2009. Disruption of vertical motility by shear triggers formation of thin phytoplankton layers. Science 323 (5917), 1067–1070.

Edwards, K.P., Hare, J.A., Werner, F.E., Seim, H., 2007. Using 2-dimensional dispersal kernels to identify the dominant influences on larval dispersal on continental shelves. Mar. Ecol. Prog. Ser. 352, 77–87.

Egbert, G.D., Bennett, A.F., Foreman, M.G., 1994. TOPEX/POSEIDON tides estimated using a global inverse model. J. Geophys. Res. 99 (C12), 24821–24852. http://dx.doi.org/10.1029/94JC01894.

Egbert, G.D., Ray, R.D., 2001. Estimates of M_2 tidal energy dissipation from TOPEX/POSEIDON altimeter data. J. Geophys. Res. 106 (C10), 22475–22502. http://dx.doi.org/10.1029/2000JC000699.

Ehrlich, M.D., Ciechomski, J.D., 1994. Reseña sobre la distribución de huevos y larvas de merluza (*Merluccius hubbsi*) basada en veinte años de investigaciones. Frente Marít. 15, 37–50.

Ehrlich, M.D., Martos, P., Madirolas, A., Sánchez, R.P., 2000. Causes of spawning pattern variability of anchovy and hake on the Patagonian shelf. In: ICES Council Meeting, vol. 6, pp. 1–13.

Franco, B.C., 2013. Procesos acoplados bento-pelágicos relacionados con el establecimiento y deriva larval de la vieira patagónica (*Zygochlamys patagonica*) en el Océano Atlántico sudoeste (Ph.D. thesis). Universidad de Buenos Aires, Argentina (unpublished).

Gardiner, C.W., 1983. Handbook of Stochastic Methods. Springer-Verlag, Berlin, p. 432.

Glorioso, P.D., 1987. Temperature distribution related to shelf-sea fronts on the Patagonian shelf. Cont. Shelf Res. 7 (1), 27–34.

Glorioso, P.D., Flather, R.A., 1997. The Patagonian shelf tides. Prog. Oceanogr. 40, 263–283.

Hunter, J.R., Craig, P.D., Phillips, H.E., 1993. On the use of random walk models with spatially variable diffusivity. J. Comput. Phys. 106, 366–376.

Kloeden, P.E., Platen, E., 1999. Numerical Solution of Stochastic Differential Equations. Springer-Verlag, Berlin, 636 pp.

Large, W.G., Gent, P.R., 1999. Validation of vertical mixing in an equatorial ocean model using large eddy simulations and observations. J. Phys. Oceanogr. 29, 449–464.

Ledwell, J.R., Watson, A.J., Law, C.S., 1998. Mixing of a tracer in the pycnocline. J. Geophys. Res. 103, 21499–21529.

Marchesiello, P., McWilliams, J.C., Shchepetkin, A., 2001. Open boundary conditions for long-term integration of regional oceanic models. Ocean Model. 3, 1–20.

Mauna, A.C., Botto, F., Franco, B., Schwartz, J.M., Acha, E.M., Lasta, M.L., Iribarne, O.O., 2011. Shifts in an epibenthic trophic web across a marine frontal area in the Southwestern Atlantic (Argentina). J. Sea Res. 66 (3), 248–255.

Milstein, G.N., 1974. Approximate integration of stochastic differential equations. In: Theory of Probability and its Applications, vol. 19, pp. 557–562.

North, E.W., Hood, R.R., Chao, S.-Y., Sanford, L.P., 2005. The influence of episodic events on transport of striped bass eggs to an estuarine nursery area. Estuaries 28 (1), 106–121.

North, E.W., Hood, R.R., Chao, S.-Y., Sanford, L.P., 2006. Using a random displacement model to simulate turbulent particle motion in a baroclinic frontal zone: a new implementation scheme and model performance tests. J. Mar. Syst. 60, 365–380.

Orensanz, J.M., Parma, A.M., Turk, T., Valero, J., 2006. Dynamics, assessment and management of exploited natural populations. In: Shumway, S.E. (Ed.), Scallops: Biology, Ecology and Aquaculture, second ed. Elsevier, Amsterdam, pp. 765–868.

Pájaro, M., Macchi, G.J., Martos, P., 2005. Reproductive pattern of the Patagonian stock of Argentine hake (*Merluccius hubbsi*). Fish. Res. 72, 97–108.

Palma, E.D., Matano, R.P., Piola, A.R., 2004. A numerical study of the Southwestern Atlantic Shelf circulation: barotropic response to tidal and wind forcing. J. Geophys. Res. 109, C08014. http://dx.doi.org/10.1029/2004JC002315.

Pisoni, J.P., Rivas, A.L., Piola, A.R., 2014. On the variability of tidal fronts on a macrotidal continental shelf, Northern Patagonia, Argentina. Deep-Sea Res. Part II Top. Stud. Oceanogr. http://dx.doi.org/10.1016/j.dsr2.2014.01.019 (in press).

Rivas, A.L., 1994. Spatial variation of the annual cycle of temperature in the Patagonian shelf between 40 and 50° of south latitude. Cont. Shelf Res. 14, 1539–1554.

Rivas, A.L., 1997. Current-meter observations in the Argentine Continental Shelf. Cont. Shelf Res. 17, 391–406.

Rivas, A.L., Dogliotti, A.I., Gagliardini, D.A., 2006. Seasonal variability in satellite-measured surface chlorophyll in the Patagonian Shelf. Cont. Shelf Res. 26, 703–720.

Risien, C.M., Chelton, D.B., 2008. Global climatology of wind stress and wind stress derivative fields from 7 years of QuikSCAT scatterometer data. J. Phys. Oceanogr. 38, 2379–2413.

Rodean, H.C., 1996. Stochastic Lagrangian Models of Turbulent Diffusion. In: Meteorological Monographs, vol. 48. American Meteorology Society, Boston, MA, 84 pp.

Ross, O.N., Sharples, J., 2004. Recipe for 1-d Lagrangian particle tracking models in space-varying diffusivity. Limnol. Oceanogr. Methods 2, 289–302.

Ross, O.N., 2006. Particles in motion: how turbulence affects Plankton sedimentation from an oceanic mixed layer. Geophys. Res. Lett. 33, L10609. http://dx.doi.org/10.1029/2006GL026352.

Sabatini, M.E., Martos, P., 2002. Mesozooplankton features in a frontal area off northern Patagonia (Argentina) during spring 1995 and 1998. Sci. Marít. 66, 215–232.

Schejter, L., Bremec, C., Akselman, R., Hernández, D., Spivak, E., 2002. Annual feeding cycle of the Patagonian scallop *Zygochlamys patagonica* (King and Broderip, 1832) in Reclutas bed (39S–55W), Argentine Sea. J. Shellfish Res. 21, 553–559.

Schlag, Z.R., North, E.W., Smith, K.A., 2008. Larval TRANSport Lagrangian Model (LTRANS) User's Guide. Technical Report of the University of Maryland Center for Environmental Science Horn Point Laboratory. Cambridge, MD. 146 pp.

Sentchev, A., Korotenko, K., 2007. Modelling distribution of flounder larvae in the eastern English channel: sensitivity to physical forcing and biological behavior. Mar. Ecol. Prog. Ser. 347, 233–245.

Shchepetkin, A.F., McWilliams, J.C., 2005. The regional oceanic modeling system (ROMS): a split-explicit, free-surface, topography-following-coordinate oceanic model. Ocean Model. 9, 347–404.

Siegel, D.A., Kinlan, B.P., Gaylord, B., Gaines, S.D., 2003. Lagrangian descriptions of marine larval dispersion. Mar. Ecol. Prog. Ser. 260, 83–96.

Simpson, J.H., 1981. The shelf-sea fronts: implications of their existence and behavior. Philos. Trans. R. Soc. Lond. Ser. A Math. Phys. Sci. 302, 531–546.

Simpson, J.H., Bowers, D., 1981. Models of stratification and frontal movement in shelf seas. Deep-Sea Res. Part A 28, 727–738.

Simpson, J.H., Souza, A.J., 1995. Semidiurnal switching of stratification in the region of freshwater influence of the Rhine. J. Geophys. Res. 100, 7037–7044.

Simpson, J.H., 1998. Tidal processes in shelf seas. In: The sea, vol. 10, pp. 113–150.

Stijnen, J.W., Heemink, A.W., Lin, H.X., 2006. An efficient 3D particle transport model for use in stratified flow. Int. J. Numer. Methods Fluids 51, 331–350.
Tonini, M.H., Palma, E.D., Piola, A.R., 2013. A numerical study of gyres, thermal fronts and seasonal circulation in austral semi-enclosed gulfs. Cont. Shelf Res. 65, 97–110. http://dx.doi.org/10.1016/j.csr.2013.06.011.
Visser, A.W., 1997. Using random walk models to simulate the vertical distribution of particles in a turbulent water column. Mar. Ecol. Prog. Ser. 158, 275–281.
Werner, F.E., Perry, R.I., Lough, R.G., Naimie, C.E., 1996. Trophodynamic and advective influences on Georges Bank larval cod and haddock. Deep-Sea Res. 43, 1793–1822.
Werner, F.E., MacKenzie, B.R., Perry, R.I., Lough, R.G., Naimie, C.E., Blanton, B.O., Quinlan, J.A., 2001. Larval trophodynamics, turbulence, and drift on Georges Bank: a sensitivity analysis of cod and haddock. Sci. Mar. 65, 99–115.